

ORIGINAL ARTICLE

Pressure Drop of Partially Blocked Hagen-Poiseuille Flow using CFD Simulation

B. Tantoro¹, W. Y. Tey^{1,2*} and W. Y. H. Ryan¹¹Department of Mechanical Engineering, Faculty of Engineering, UCSI University, Kuala Lumpur, Malaysia²Takasago i-Kohza, Malaysia-Japan International Institute of Technology Malaysia, Universiti Teknologi Malaysia, Kuala Lumpur, Malaysia

ABSTRACT – Piping serves as an important pillar in most of the engineering applications while the quantification on the pressure drop due to various factors is always the central issue of efficient piping maintenance and design. In most of the previous studies, fluid flow at sudden expansion and contraction was studied separately. Indeed, the flow characteristics for an internal flow in which both expansion and contraction co-exist within a short distance is not well studied. Such flow is indeed a blocked internal flow. In this study, the effect of the percentage of blockage to the velocity field and power loss in Hagen-Poiseuille flow is investigated. The current work found that using the conventional way of minor losses analysis, the energy loss is over-estimated because in a close contraction-expansion region, the flow is not able to be fully developed. The equation of minor losses due to internal blockage is re-computed too. The study is executed using the standard $k-\epsilon$ model assisted by CFD commercial software of ANSYS Fluent.

ARTICLE HISTORYRevised: 21st Aug 2019Accepted: 30th Sept 2019**KEYWORDS**

Engineering piping; Piping blockage; Pressure drop; Internal flow; Hagen-Poiseuille flow; Computational fluid dynamics

INTRODUCTION

Investigation on pressure drop of internal flow is an instrumental topic in various engineering applications such as civil piping [1], air-conditioning system [2] and biomedical analysis [3,4]. The pressure drop due to the head loss based on Colebrook-White equation well has studied in many works of literature [5,6]. However, in real-world, there are many more factors that contribute to the abnormal pressure drop, which comprise filtration intensity [7,8], portion of impurities [9], pipe bending [10,11], fluid-phase ratio [12,13], geometry of pipe [14,15] and internal blockage [16,17], and their room of research remains spacious. In many engineering designs, the reduction of flow cross-sectional area is required to serve the relevant purposes such as orifice flowmeter, heat exchanger, chemical reactor and biomedical tubes. Such a reduction can be regarded as internal blockage, which shall alter the pressure drop and the power waste.

Nguyen et al. [16] investigated the thermal and flow behaviour at the wake of the blocked flow. They divided the wake region into separation region, reattachment point, recovery region and fully recovered region as shown in Figure 1. The experiment on pressure drop due to porous blockages was conducted by Anuar et al. [17], Swanson et al. [18] and Pourfarzad et al. [19]. Meanwhile, Cha [20] and Aly et al. [21] studied the pressure drop of a circular pipe due to different fractal-shaped orifices and they found that such specially designed orifices will reduce the pressure drop. Tey and Kang [22] also found that the lesser the number of edges for polygonal pipe, the larger the power loss. Numerical simulation was conducted too by Gorman et al. [23] to observe how the blockage at the inlet of a bent pipe influences the pressure drop. The alteration of internal flow behaviour due to bluff body intrusion is scrutinised by Venugopal et al. [24] and Kumar et al. [25]. Further results on pressure drop due to a moving blockage was reported too by Li et al. [26].

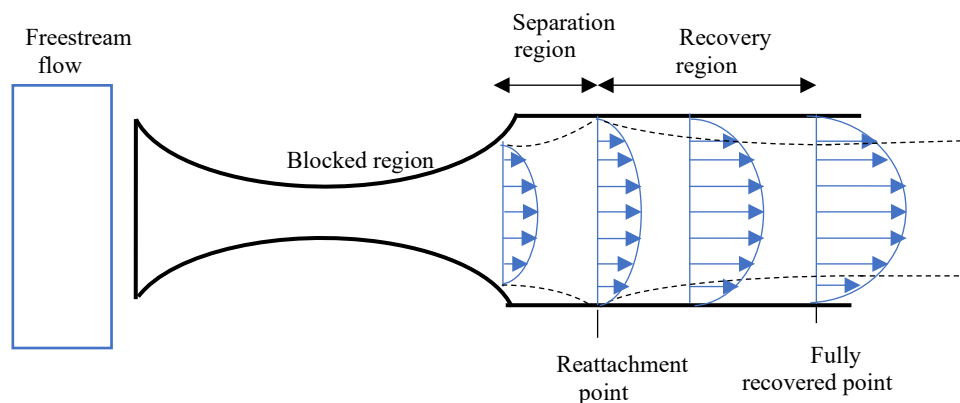


Figure 1. Schematic diagram for the velocity profile at the wake of blocked flow.

The blockage in an internal flow can be regarded as a form of “pipe fittings and transitions” in which its head loss h_L can be expressed as a function of loss coefficient, average flow velocity and gravitational acceleration [27]. Although the velocity profile will be recovered after some distance away from the flow blockages, the formation of eddies or flow separation region will consume some of the flow energy. Many fluid mechanics textbooks [27-29] discussed the loss coefficient in details.

The loss coefficient of blocked internal flow can be estimated by combining the loss coefficient due to sudden expansion and contraction of the pipe. The equation is limited by some cases especially when the ratio between the smaller and larger cross-sectional area is approaching zero or infinity. Moreover, the short distance between the contraction and expansion orifice may disturb the recovery of flow, and this will alter some changes on pressure drop. A number of researches [30-33] have been done on the effects of sudden contraction or expansion based on some case studies, yet the effect of blockage ratio to the pressure drop is not systematically quantified and studied so far. The information is required for blockage prediction and piping design whenever a choking of pipe cross-sectional area is required.

Hence, the objective of the paper is to quantify the effect of blockage percentage to the pressure drop, power waste and velocity field of the flow. The minor losses incurred by the blockage will be re-examined too. The standard $k-\epsilon$ is applied with the assistance of commercial software ANSYS Fluent. Our study is based on Hagen-Poiseuille flow, which is indeed the benchmark problem [18] for further experimental and numerical analysis.

COMPUTATIONAL MODELLING AND METHODOLOGY

A circular pipe is constructed with the blockage percentage from 5% to 95% with 5% increment for each case study. The pipe is divided into three sections: the inlet section, blockage section and outlet section, in which their length is set as 30 cm, 100 cm and 100 cm respectively, as shown in Figure 2.

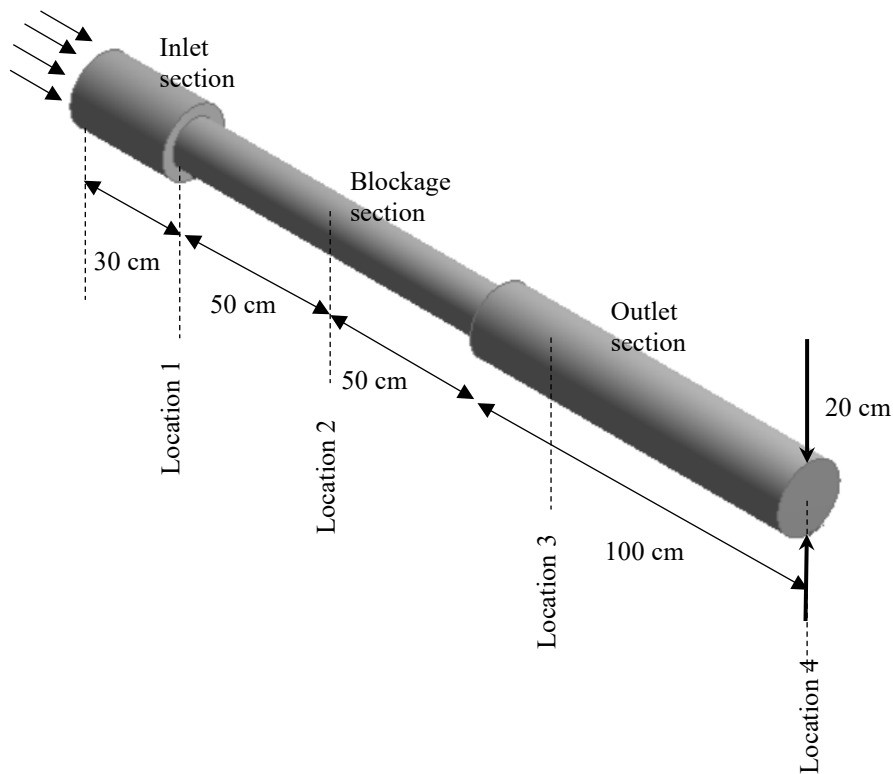


Figure 2. Physical modelling of blocked Hagen-Poiseuille flow.

Due to the effect of flow turbulence, application of incompressible Time-Averaged Continuity and Navier-Stokes equations is suitable for our simulation [34]. The governing in tensor form can be written as in Eq. (1) and (2).

$$\frac{\partial \bar{u}_i}{\partial x_i} = 0 \tag{1}$$

$$\rho \frac{\partial (\bar{u}_i \bar{u}_j)}{\partial x_j} = -\frac{\partial \bar{P}}{\partial x_i} + \frac{\partial}{\partial x_j} \left[\mu \left(\frac{\partial \bar{u}_i}{\partial x_j} + \frac{\partial \bar{u}_j}{\partial x_i} \right) \right] + \frac{\partial \tau_{ij}}{\partial x_j} \tag{2}$$

The last term of Eq.(2) represents the Reynolds stresses, meanwhile \bar{u} and \bar{P} signifies the unsteady velocity and pressure fluctuation respectively with an assumption of isotropic condition. This will create three extra unknowns and in order to close the equation, the k -epsilon model [35] is applied. In this turbulent model, the turbulent kinetic energy (k) and dissipation rate (ϵ) is used to replace velocity of the axis component. Upon modification, the k -equation and ϵ -equation can be expressed as in Eq.(3) and (4).

$$\rho \left(\frac{\partial \bar{k}}{\partial t} + \frac{\partial (\bar{k} \bar{u}_j)}{\partial x_j} \right) = \frac{\partial}{\partial x_j} \left[\left(\mu + \frac{0.09 \rho \bar{k}^2}{\bar{\epsilon} \sigma_k} \right) \frac{\partial \bar{k}}{\partial x_j} \right] - \left(\frac{2}{3} \rho \bar{k} \delta_{ij} \frac{\partial \bar{u}_i}{\partial x_j} \right) - \rho \bar{\epsilon} \tag{3}$$

$$\rho \left(\frac{\partial \bar{\epsilon}}{\partial t} + \frac{\partial (\bar{\epsilon} \bar{u}_j)}{\partial x_j} \right) = \frac{\partial}{\partial x_j} \left[\left(\mu + \frac{0.09 \rho \bar{k}^2}{\bar{\epsilon} \sigma_\epsilon} \right) \frac{\partial \bar{\epsilon}}{\partial x_j} \right] - 1.44 \frac{\bar{\epsilon}}{\bar{k}} \left(\frac{2}{3} \rho \bar{k} \delta_{ij} \frac{\partial \bar{u}_i}{\partial x_j} \right) - 1.92 \frac{\rho \bar{\epsilon}}{\bar{k}} \tag{4}$$

where δ_{ij} is the Kronecker delta, while σ_k and σ_ϵ are empirical constants. The model is widely applied in many turbulence modelling [36,37], and it is proven as a reliable technique for turbulent flow simulation. In the numerical setting, the semi-implicit pressure-linked equations - consistent (SIMPLEC) algorithm is applied. SIMPLEC algorithm is a pressure-velocity coupling scheme proposed by Van Doormal and Raithby [38] for steady flow computation. The algorithm is improvised from the convectional SIMPLE algorithm, which was put forward by Patankar and Spalding [39] for coupling problem. In SIMPLEC algorithm, the residuals surrounding the node of interest will be included too in the computation of momentum equation for the sake of mathematical consistency. In fact, SIMPLEC algorithm is a popular coupling scheme, which has been widely applied in computational fluid dynamics [40,41]. The second-order upwind scheme is applied for the convection term, turbulent kinetic energy and dissipation rate; meanwhile, the first-order implicit method is deployed for transient formulation. The under-relaxation factor for pressure and k - ϵ term is 0.3 and 0.7 respectively.

The simulation is conducted by using water at 20°C as the fluid medium, in which its density and dynamic viscosity of 998.2 kg/m³ and 0.001003 kg/ms respectively. The diameter and total pipe length are 20 cm and 2.5 m respectively, with the wall roughness of 0.5. The inlet velocity is set at 0.51 m/s, which corresponds to Reynolds number of 10⁵. The outlet of the pipe is the location at Location 4.

In our model, the tetrahedron patch conforming meshing scheme is applied. The outer wall boundaries are set using inflation technique with minimum 20 layers of the boundary layer, 0.272 transition ratio and 1.2 growth rate. This will ensure a better mesh resolution to resolve the boundary layer and flow recirculation. Upon a mesh independence study as illustrated in Table 1, the element size we used is 0.0118 m. The study is conducted based on the velocity field at the middle of the pipe at four different locations as shown in Figure 1. The resulting mesh can be shown in Figure 3. Upon the simulation, the average pressure ($P_{out,ave}$) at the exit of the pipe, or Location 4, can be analysed via Eq. (5).

The mesh independence study is also conducted, as shown in Table 1. The value of fluid velocity is recorded at four different locations of the pipe, which have been referred in Figure 2. Upon the element size as small as 0.012 or elements number above 474181, the results will converge.

$$P_{out,ave} = \frac{\sum P_{out}}{n} \tag{5}$$

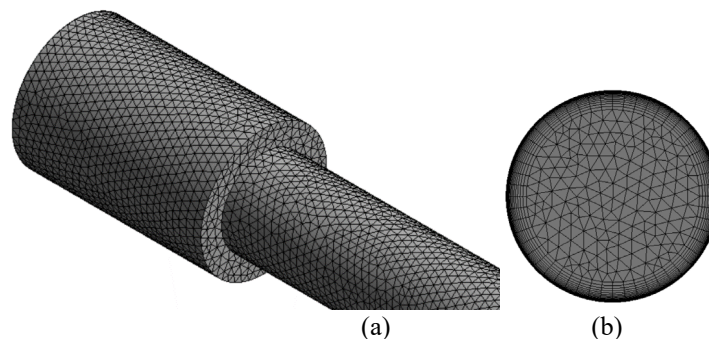


Figure 3. The meshing on the problem domain where (a) tetrahedron mesh and (b) improved near-wall inflated mesh is applied.

Table 1. Velocity at varied location due to different element size.

Element size (m)	No of elements	Location 1	Location 2	Location 3	Location 4
0.0160	301619	5.3214	6.5908	5.9685	2.5730
0.0150	327284	5.3468	6.5878	5.9710	2.4841
0.0140	360686	5.3122	6.4077	5.9885	2.6384
0.0130	404047	5.3888	6.5906	5.9656	2.7390
0.0120	457476	5.4449	6.5790	5.9610	2.8782
0.0118	474181	5.4021	6.5589	5.9655	2.9664
0.0115	491436	5.3974	6.5555	5.9538	2.8990

RESULTS AND DISCUSSION

The schematic illustrations of the effect of blockage percentage on the velocity profile can be shown in Figure 4. The flow fields are captured at the end of the pipe (Location 4), where the flow is under-recovery stage, i.e. the velocity profile resembles the conventional Hagen-Poiseuille flow without any discontinuity. The larger the percentage of blockage, the less parabolic shape that the profile shows, and this proved that the blockage increases the flow turbulent.

The velocity contour due to different percentage of blockage is showed in Figure 5. Generally, there is a sudden increment of velocity at the shrinkage region (Location 1), while the velocity decreases gradually after the orifice (Location 3). From 5% to 30% of blockages, the velocity is still able to be fully developed inside the shrank tube. However, upon 30%, the fluid needs to travel out from the shrank tube despite underdeveloped. It is noticeable too that at a high percentage of blockages, the velocity fluctuation is observed, and the flow is highly unstable. The effect of energy loss coefficient or pressure drop due to the percentage of blockage can be shown in Figure 6. The equation of energy loss coefficient (W_{loss}) and percentage of blockage (α) can be defined respectively as in Eq. (6) and (7).

$$W_{loss} = \frac{P_{blocked} - P_{full}}{P_{full}} \tag{6}$$

$$\alpha = \frac{A_L - A_S}{A_L} \times 100\% \tag{7}$$

where $P_{blocked}$, P_{full} , A_S and A_L is the pressure drop due to blocked pipe, pressure drop due to unblocked pipe, the smaller cross-sectional area of the pipe and larger cross-sectional area of the pipe.

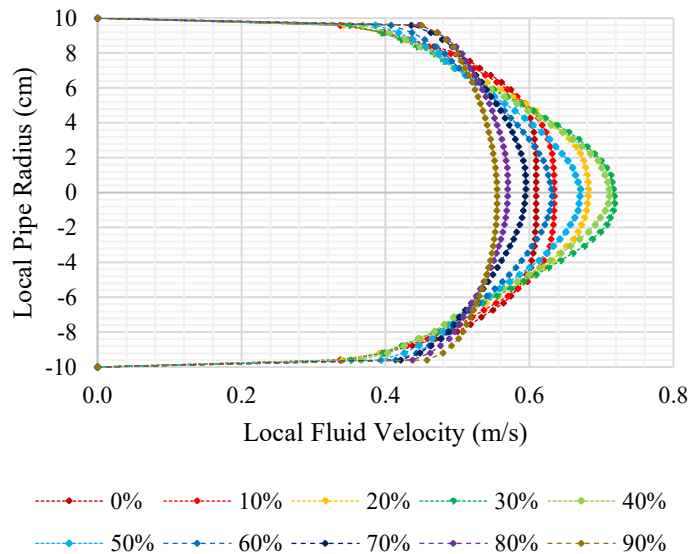


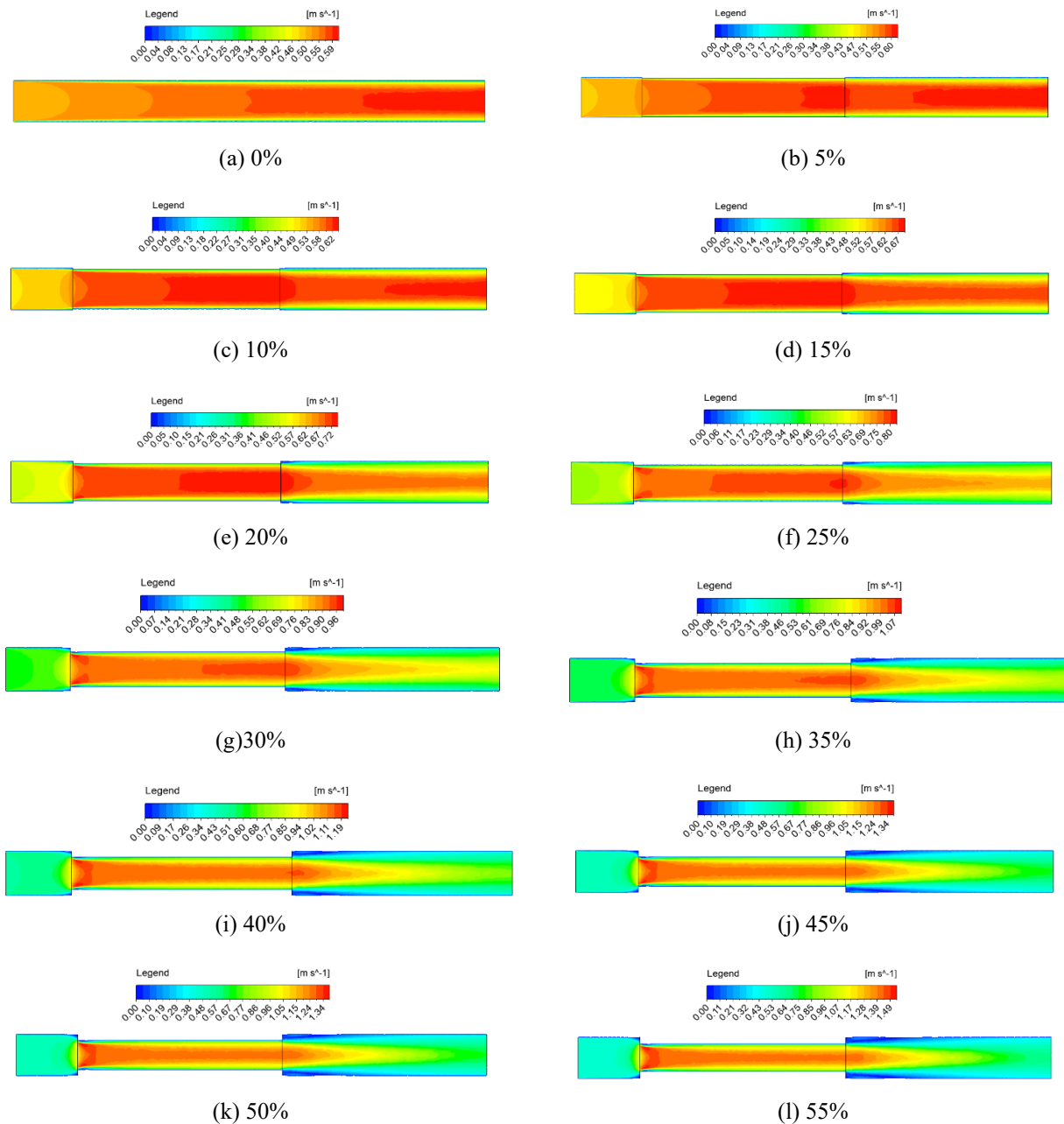
Figure 4. The velocity profile at the wake of the pipe flow due to a different percentage of blockages at Location 4.

Due to the regression accuracy, the mathematical relationship between the blockage and energy loss coefficient is divided into five piecewise equations. The larger the blockage, the more sensitive the energy loss, i.e. an increase of blockage percentage resulted in a higher rate of energy loss increment. The correlation appears in a piecewise manner to ensure a higher coefficient of determination and accuracy across α , as in Eq. (8).

$$W_{loss} = \begin{cases} 0.002\alpha^2 - 0.0015\alpha + 0.0518 & 5\% \leq \alpha \leq 25\% & (8.1) \\ 0.0074\alpha^2 - 0.3367\alpha + 5.0895 & 25\% \leq \alpha \leq 50\% & (8.2) \\ 0.0476\alpha^2 - 4.5904\alpha + 117.44 & 50\% \leq \alpha \leq 70\% & (8.3) \\ 0.6172\alpha^2 - 86.904\alpha + 3090.2 & 70\% \leq \alpha \leq 85\% & (8.4) \\ 2 \times 10^{-7} \exp(0.2402\alpha) & 85\% \leq \alpha \leq 95\% & (8.5) \end{cases}$$

The coefficient of determination of Eq. (8.1) to (8.5) is 0.9997, 0.9995, 0.9994, 0.9956 and 0.9835 respectively. The graphical plots if these correlations can be demonstrated in Figure 6. Eq. (8.1) to (8.5) can be further generalised into Eq. (9), where C_4, C_3, C_2, C_1 and C_0 is the loss constant of $2 \times 10^{-7}, -2 \times 10^{-5}, 1.7 \times 10^{-3}, 0.0107$ and 0.6951 , with coefficient of determination of 0.9967. The plot of Eq. (9) can be shown in Figure 7. It can be clearly observed that the gradient of energy loss coefficient keeps increasing in an fourth order exponential way.

$$W_{loss}^{1/5} = C_4\alpha^4 + C_3\alpha^3 + C_2\alpha^2 + C_1\alpha^1 + C_0 \tag{9}$$



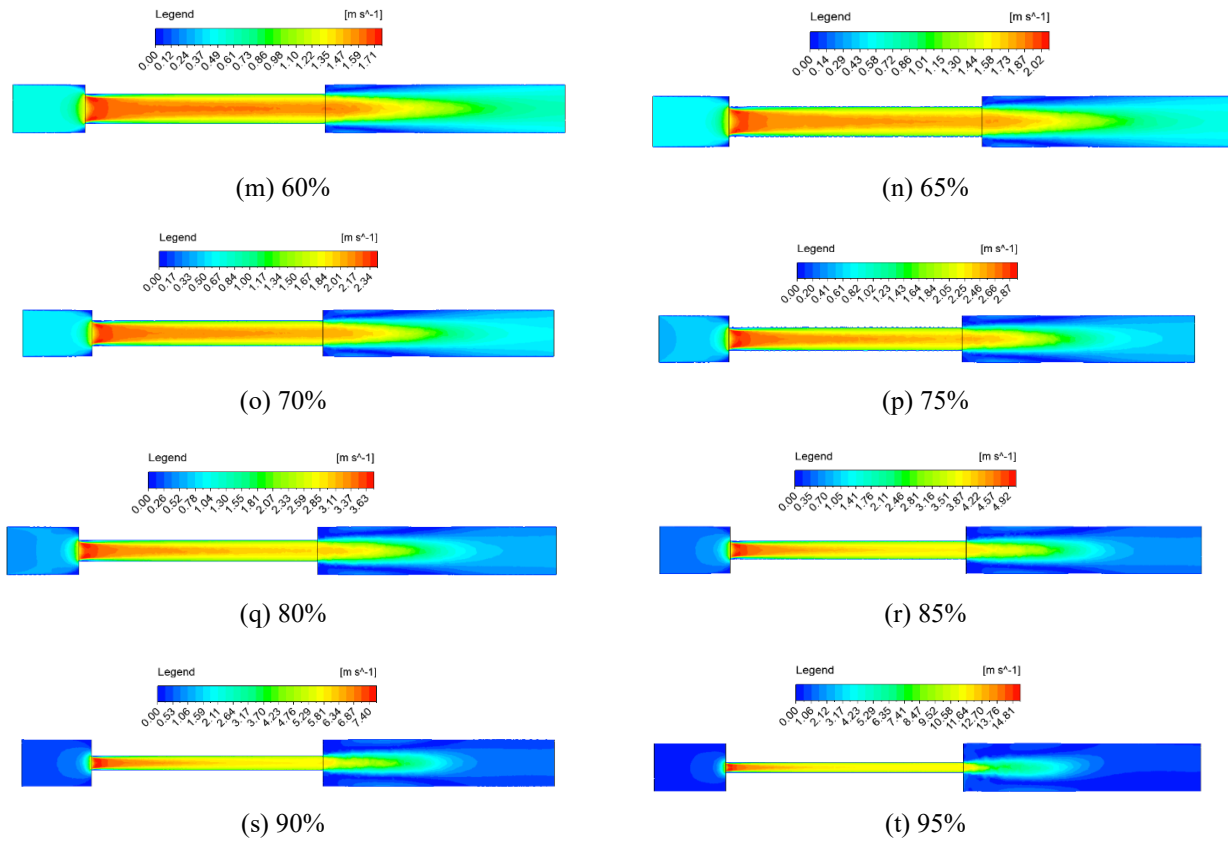
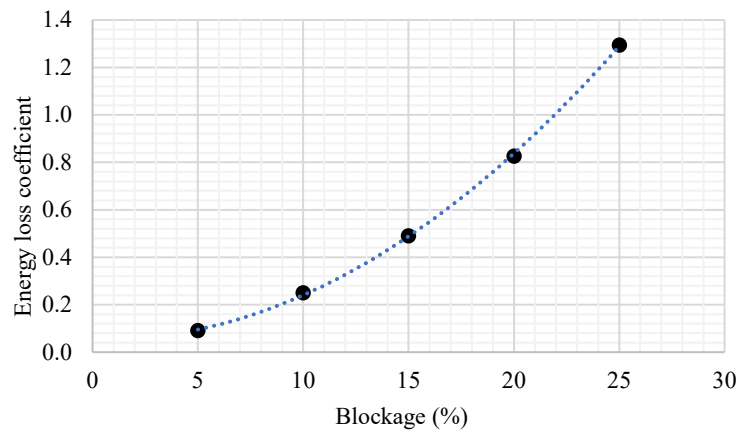
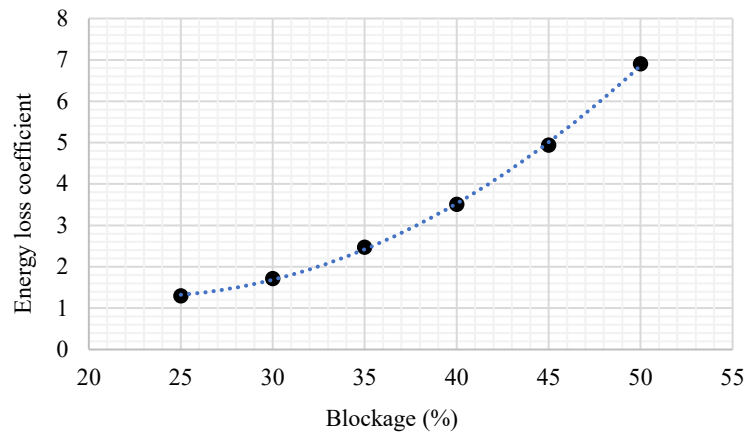


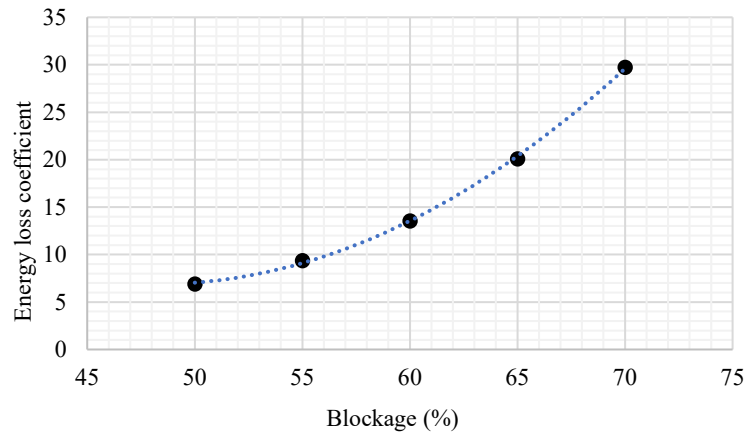
Figure 5. The velocity contour at different percentage of blockage.



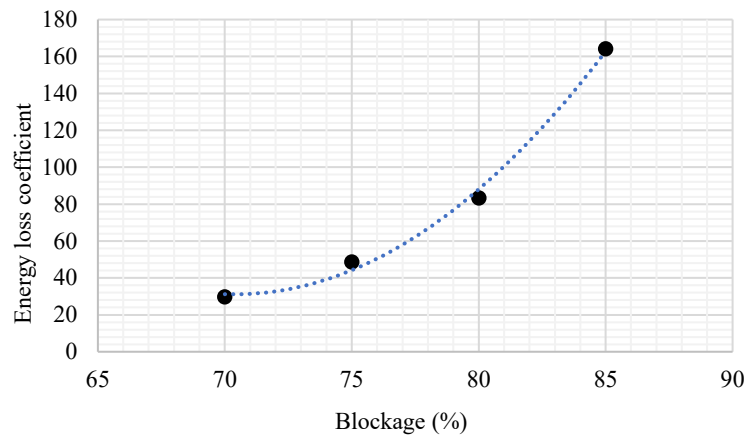
(a)



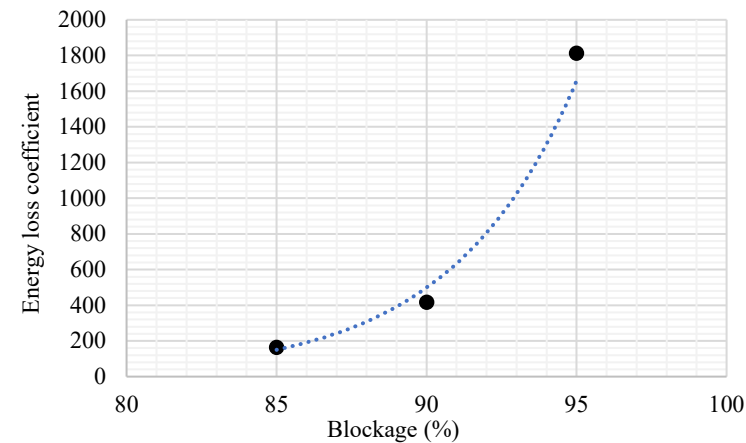
(b)



(c)



(d)



(e)

Figure 6. Relationship between percentage of blockage and energy loss coefficient when the percentage of blockage is: (a) 5%-25%; (b) 25%-50%; (c) 50%-70%; (d) 70%-85%; and (e) 85%-95%.

Validation process is done by comparing the simulated results and the theoretical results by presuming the flow friction is composed of major and minor losses. The major losses are indeed the Darcy friction factor, computed through Eq. (10) via the hybrid techniques as proposed by Tey et al. [6]. Zero relative roughness is applied. Meanwhile the values of minor losses (sudden contraction and expansion) are computed using bilinear interpolation method [43]. The theoretical energy loss coefficient can be therefore defined as in Eq. (11).

$$\frac{1}{\sqrt{f}} = -2 \log \left(\frac{\varepsilon / D}{3.71} + \frac{2.51}{\text{Re} \sqrt{f}} \right) \tag{10}$$

$$W_{\text{loss}} = \frac{f \frac{L}{D} \frac{\rho v^2}{2} - P_{\text{theoretical}}}{P_{\text{theoretical}}} \tag{11}$$

in which, $P_{\text{theoretical}} = \frac{\rho}{2} \left[\left(\frac{fLv^2}{D} \right)_{\text{inlet}} + \left(\frac{fLv^2}{D} \right)_{\text{blockage}} + \left(\frac{fLv^2}{D} \right)_{\text{outlet}} + (\sum K)(v^2)_{\text{blockage}} \right]$, where K is the minor loss coefficient due to sudden expansion and contraction.

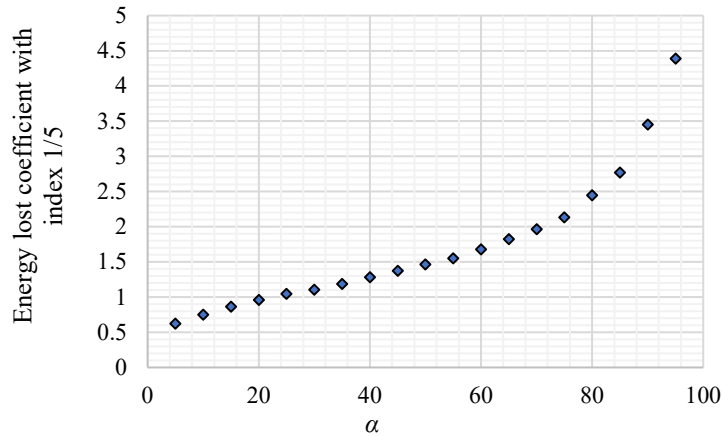


Figure 7. Relationship between power loss with index 1/5 and percentage of blockage in an internal flow.

The theoretical pressure drop is indeed contributed by all the minor losses and the head loss of the normal and blocked sections. The curve of theoretical energy loss coefficient generally follows the exponential trend of the computed value, as in Figure 8. However, the theoretical energy loss overestimates the computed value by about 2.35 times. This is ascribable to the reason that in theoretical works, the effect of distance between the contraction and expansion is not considered, as shown in Figure 9.

In the theoretical framework, the loss is contributed by the fully developed vorticity and fully developed as described in [10,16,42]. Nonetheless in current work, the contraction and expansion region are located close within each other and the reattachment is not able to fully formed at the contracted region. This indeed will decrease the minor loss incurred. Therefore, the value of minor losses for the case of blocked flow (close sudden contraction and expansion) is re-computed and proposed here too for possible future investigation. Figure 10 illustrates the relationship between K and the percentage of blockage, and they can be correlated via Eq. (12) with an excellent coefficient of determination of 1.

$$K = 10^{-4} \left(-\frac{\alpha^5}{10^7} + \frac{\alpha^4}{5 \times 10^4} - \frac{\alpha^3}{500} + \frac{\alpha^2}{100} + 7\alpha + 3 \right) \tag{12}$$

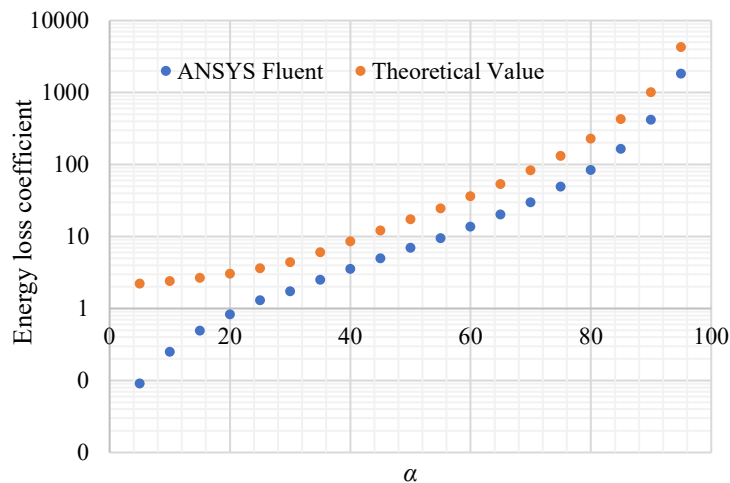


Figure 8. Comparison of the energy loss coefficient obtained using ANSYS Fluent and theoretical computation.

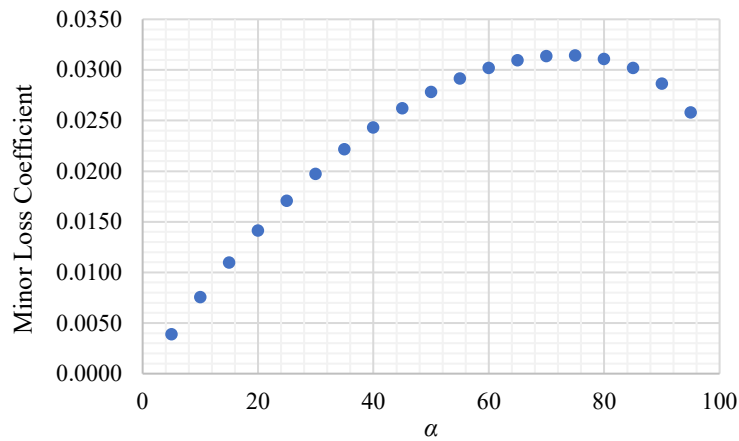


Figure 9. Re-computation of minor loss coefficient versus the percentage of blockage for a blocked Hagen-Poiseuille flow.

CONCLUSION

The simulation of partially blocked Hagen-Poiseuille flow is conducted numerically using SIMPLEC algorithm. The computed energy loss increases exponentially in accordance with the theoretical calculation. However, since the existing theoretical framework studies the contraction and expansion separately without considering the full formation of vorticity, the theoretical value will over-estimate the energy loss. An equation for minor losses with respect to the percentage of blockage for blocked Hagen-Poiseuille flow is proposed too for future investigation.

ACKNOWLEDGEMENT

This research is supported by Pioneer Scientist Incentive Fund (PSIF) with grant number Proj-In-FETBE-038, Centre of Excellence for Research, Value Innovation and Entrepreneurship (CERVIE), UCSI University Kuala Lumpur, Malaysia.

REFERENCES

- [1] Qi F and Liu CJ. A novel engineering evaluation for pressure piping containing circumferential defects. *Procedia Engineering* 2015; 130: 1719-1729.
- [2] Yokohama R, Kitano H and Wakui T. Optimal operation of heat supply systems with piping networks. *Energy* 2017; 137: 888-897.
- [3] Zhou Y, Lee C and Wang J. Computational fluid dynamics analyses on hemodynamic characteristics in stenosed arterial models. *Journal of Healthcare Engineering* 2018; 2018: 4312415.
- [4] El-Bouri WK and Payne SJ. Investigating the effects of a penetrating vessel occlusion with a multi-scale microvasculature model of the human cerebral cortex. *NeuroImage* 2018; 172: 94-106.
- [5] Yildirim G. Computer-based analysis of explicit approximations to the implicit Colebrook-White equation in turbulent flow friction factor calculation. *Advances in Engineering Software* 2009; 40: 1183-1190.
- [6] Tey WY, Tan LK and Ang CK. A highly computationally efficient explicit-iterative hybrid algorithm for Colebrook-White equation. In: *7th International Conference on Software and Computer Application*, pp. 269-273; 2018.
- [7] Daniel RC, Billing JM, Russell RL, Shimskey RW, Smith HD and Peterson RA. Integrated pore blockage-cake filtration model for crossflow filtration. *Chemical Engineering Research and Design* 2011; 89: 1094-1103.
- [8] Yang H, He S, Ouyang H, Anderson MJ, Shen L, and Hogan Jr CJ. The pressure drop across combined polydisperse spherical particle - Cylindrical fiber networks. *Chemical Engineering Science* 2018; 192: 634-641.
- [9] Jiang F, Zhuo P, Qi G, Li N, Bian Y, Li H, Jiang T, Li X, and Yu C. Pressure drop in horizontal multi-tube liquid-solid circulating fluidized bed. *Powder Technology* 2018; 333: 60-70.
- [10] Cengel Y and Cimbala J. *Fluid Mechanics: Fundamentals and applications*. 3rd Ed. McGraw-Hill Higher Education; 2014.
- [11] Kumal B and Singh SN. Study of pressure drop in single pass U-type heat exchanger. *Experimental Thermal and Fluid Sciences* 2017; 87: 40-49.
- [12] Hamad FA, Faraji F, Santim CGS, Basha N and Ali Z. Investigation of pressure drop in horizontal pipes with different diameters. *International Journal of Multiphase Flow* 2017; 91: 120-129.
- [13] Ladosc A, and von Rohr PR. Pressure drop of two-phase liquid-liquid slug flow in square microchannels. *Chemical Engineering Science* 2018; 191: 398-409.
- [14] Ji TH, Kim SY and Hyun JM. Pressure drop and heat transfer correlations for triangular folded fin heat sinks. *IEEE Transactions on Components and Packaging Technologies* 2007; 30(1): 3-8.

- [15] Zhang J, Fletcher DF and Li W. Heat transfer and pressure drop characteristics of gas–liquid Taylor flow in mini ducts of square and rectangular cross-sections. *International Journal of Heat and Mass Transfer* 2016; 103: 45-56.
- [16] Nguyen NH, Kim J, Hong SH, Moon SK and Song CH. Improvements of COBRA-TF on the effect of flow blockage during a LB LOCA with consideration of fuel relocation phenomenon. *Nuclear Engineering and Design* 2017; 325: 218-231.
- [17] Anuar FS, Abdi IA, Odabae M and Hooman K. Experimental study of fluid flow behaviour and pressure drop in channels. *Experimental Thermal and Fluid Science* 2018; 99: 117-128.
- [18] Swanson J, Kittelson WD, Newman R and Ziebarth R. Filtration efficiency and pressure drop of miniature diesel particulate filters. *Aerosol Science and Technology* 2013; 47(4): 452-461.
- [19] Pourfarzad E, Ghadiri K, Behrangzeda A and Ashjee M. Experimental investigation of heat transfer and pressure drop of alumina–water nano-fluid in a porous miniature heat sink. *Experimental Heat Transfer* 2018; 31(6): 495-512.
- [20] Cha SC. Optimization of the heat transfer rate and pressure drop of inside profiled tubes – Part 1. *Chemical Engineering and Technology* 2005; 28(2): 204-209.
- [21] Aly AAE, Chong A, Nicolleau F and Beck S. Experimental study of the pressure drop after fractal-shaped orifices in turbulent pipe flows. *Experimental Thermal and Fluid Science* 2010; 34: 104-111.
- [22] Tey WY and Kang KS. Power loss in straight polygon pipe via CFD simulation. *Progress in Energy and Environment* 2018; 7: 1-10.
- [23] Gorman JM, Sparrow EM, Smith CJ, Ghosh A, Abraham JP, Daneshfaraz R and Joudi AR. In-bend pressure drop and post-bend heat transfer for a bend with a partial blockage at its inlet. *Numerical Heat Transfer Part A: Applications* 2018; 73(11): 743-767.
- [24] Venugopal A, Agrawal A and Prabhu SV. Influence of blockage and shape of a bluff body on the performance of vortex flowmeter with wall pressure measurement. *Measurement* 2011; 44: 954-964.
- [25] Kumar A, Chauhan R, Kumar R, Singh T, Sethi M, Kumar A and Sharma A. Developing heat transfer and pressure loss in an air passage with multi discrete V-blockages. *Experimental Thermal and Fluid Science* 2017; 84: 266-278.
- [26] Li W, Lu S, Liu Y, Wang R, Huang Q and Yan J. CFD simulation of the unsteady flow of a single coal log in a pipe. *The Canadian Journal of Chemical Engineering* 2015; 93(11): 2084-2093.
- [27] Munson BR, Young DF and Okiishi TH. *Fundamentals of Fluid Mechanics*. 5th Ed. John Wiley & Sons Inc; 2006.
- [28] Sultanian BK. *Fluid Mechanics: An Intermediate Approach*. CRC Press; 2016.
- [29] Hibbeler RC. *Fluid Mechanics*. Pearson Education; 2017.
- [30] Balakhrisna T, Ghosh S, Das S and Das PK. Oil–water flows through sudden contraction and expansion in a horizontal pipe – Phase distribution and pressure drop. *International Journal of Multiphase Flow* 2010; 36: 13-24.
- [31] Mika L. Energy losses of ice slurry in pipe sudden contractions. *Experimental Thermal and Fluid Science* 2011; 35: 939-947.
- [32] Kaushik VVR, Ghosh S, Das G and Das PK. CFD simulation of core annular flow through sudden contraction and expansion. *Journal of Petroleum Science and Engineering* 2012; 86-87: 153-164.
- [33] Kawahara A, Mansour MH, Sadatomi M, Law WZ, Kurihara H and Kusumaningsih H. Characteristics of gas–liquid two-phase flows through a sudden contraction in rectangular microchannel. *Experimental Thermal and Fluid Science* 2015; 66: 243-253.
- [34] Tey WY, Asako Y, Sidik NAC and Goh RZ. Governing equations in computational fluid dynamics: Derivations and a recent review. *Progress in Energy and Environment* 2017; 1: 1-19.
- [35] Launder BE and Spalding DB. *Lectures in Mathematical Models of Turbulence*. Academic Press; 1972.
- [36] Guillas S, Glover N and Malki-Epshtein L. Bayesian calibration of the constants of the k- ϵ turbulence model for a CFD model of street canyon flow. *Computer Methods in Applied Mathematics and Engineering* 2014; 279: 536-553.
- [37] Liu J, Heidarinejad M, Pitchurov G, Zhang L and Srebic J. An extensive comparison of modified zero-equation, standard k- ϵ and LES models in predicting urban air flow. *Sustainable Cities and Society* 2018; 40: 28-43.
- [38] Van Doormal JP and Raithby GD. Enhancement of the SIMPLE method for predicting incompressible fluid flows. *Numerical Heat Transfer* 1984; 7: 147-163.
- [39] Patankar SV and Spalding DB. A calculation procedure for heat, mass and momentum transfer in three-dimensional parabolic flows. *International Journal of Heat and Mass Transfer* 1972; 15(10): 1787-1806.
- [40] Edalatpour M, Kianifar A and Ghiami S. Effect of blade installation on heat transfer and fluid flow within a single slope solar still. *International Communications in Heat and Mass Transfer* 2015; 66: 63-70.
- [41] Tian J, Li L, Song T, Shen C and Zhao J. Numerical study of foulant-water separation using hydrocyclones enhanced by ejection device: Effect of ejection velocity. *Energy* 2018; 163: 641-659.
- [42] Mott RL and Untener JA. *Applied Fluid Mechanics*. Pearson; 2016.
- [43] Mastyló M. Bilinear interpolation theorems and applications. *Journal of Functional Analysis* 2013; 265: 185-207.